Optical embodiments of Rabi splitting based in photonic integrated waveguide-coupled resonators

David Moss (dmoss@swin.edu.au)
Swinburne University of Technology

Research Article

Keywords: Rabi splitting, integrated photonics, optical resonators, Sagnac interference

Posted Date: January 17th, 2023

DOI: https://doi.org/10.21203/rs.3.rs-2482705/v1

Abstract

Realizing optical analogues of quantum phenomena in atomic, molecular, or condensed matter physics has underpinned a range of photonic technologies. Rabi splitting is a quantum phenomenon induced by a strong interaction between two quantum states, and its optical analogues are of fundamental importance for the manipulation of light-matter interactions with wide applications in optoelectronics and nonlinear optics. Here, we propose and theoretically investigate purely optical analogues of Rabi splitting in integrated waveguide-coupled resonators formed by two Sagnac interferometers. By tailoring the coherent mode interference, the spectral response of the devices is engineered to achieve optical analogues of Rabi splitting with anti-crossing behavior in the resonances. Transitions between the Lorentzian, Fano, and Rabi splitting spectral lineshapes are achieved by simply changing the phase shift along the waveguide connecting the two Sagnac interferometers, revealing interesting physical insights about the evolution of different optical analogues of quantum phenomena. The impact of the device structural parameters is also analyzed to facilitate device design and optimization. These results suggest a new way for realizing optical analogues of Rabi splitting based on integrated waveguide-coupled resonators, paving the way for many potential applications that manipulate light-matter interactions in the strong coupling regime.

I. Introduction

In atomic, molecular, and condensed matter physics, the response of photon-matter systems is normally characterized via spectroscopic detection of radiation by exploring physical processes like scattering, absorption, or fluorescence, resulting in spectral lineshapes that unveil the nature of the light-matter interactions [1, 2]. This interaction in a confined electromagnetic environment can be controlled to achieve a coupling regime in which coherent energy exchange occurs between light and matter. Such an exchange, in the strong light-matter coupling regime, results in anti-crossing between the atom-like emitter and the cavity-mode dispersion relations, which is described by the so-called Rabi splitting [2–4].

As a physical phenomenon arising from light-matter interactions in the strong coupling regime, Rabi splitting enables quantum coherent oscillations between the joint systems and the quantum superpositions of different quantum states. In the early 1980s, Rabi splitting was observed for many atoms [5]. Since then, it has been widely studied in a variety of quantum and semi-classical systems [2, 3, 5–11], with many applications such as enhancing or modifying the chemical landscape [12, 13], electrical conductivity [14, 15], optical nonlinearity [16], lasing [17, 18], quantum light emission [19, 20], and biological processes [21].

Optical analogues of atomic energy levels allow for the study of complex optical processes using atomic physics concepts, which have resulted in discoveries of photonic crystals (PhCs) [22], topological photonic systems [23, 24], and parity–time symmetric systems [25, 26]. In the past decade, many optical analogues of quantum phenomena have been realized, such as electromagnetically induced transparency [27–29], Fano resonances [30–35], Ramsey interference [36], Mollow triplet [37], and Rabi

splitting [38–42]. These optical analogues have been utilized in a variety of applications such as topologically protected lasers [43, 44], light storage [45–49], sensing [50–54], signal multicasting [55, 56], dispersion engineering [57, 58], structured light [59], and photonic computing [60].

In previous work, optical analogues of Rabi splitting have been realized in PhC and plasmonic cavities [6, 39, 61]. In this paper, we propose and theoretically verify a different way for realizing optical analogues of Rabi splitting based on integrated waveguide-coupled resonators. Similar to the manipulation of the interaction between different quantum states in a multi-level atomic system, the coherent mode interference in the waveguide-coupled resonator formed by two Sagnac interferometers is engineered to achieve optical analogues of Rabi splitting with anti-crossing behavior for the resonances. By changing the phase shift along the waveguide connecting the two Sagnac interferometers, transitions from symmetric Lorentzian spectral lineshape to asymmetric Fano and Rabi splitting spectral lineshapes are also achieved, showing interesting trends for the evolutions of different optical analogues of quantum phenomena. Finally, detailed analysis for the impact of device structural parameters is provided to facilitate device design and optimization. Our results theoretically confirm the effectiveness of realizing optical analogues of Rabi splitting based on integrated waveguide-coupled resonators, which offers new possibilities for many potential applications that manipulate light-matter interactions in the strong coupling regime.

Ii. Device Design And Operation Principle

As schematically illustrated in Fig. 1**(a)**, in the strong light-matter coupling regime where the coherent exchange rate of energy between light and matter is higher than the decay rate, a resonance state $|r\rangle$ (e.g., whispering gallery mode and plasmonic resonances) and a matter excitation state $|e\rangle$ (e.g., excitation states of atoms, molecules, plamons, and quantum dots) strongly couple with each other, resulting in the generation of new hybridized eigenstates separated by the Rabi splitting energy $\hbar\Omega_R$. In contrast to the original independent eigenstates, the new eigenstates arising from field-induced splitting of energy levels show a clear anti-crossing behavior in the spectral response [62], which can be exploited for manipulation of light-matter interaction that has wide applications in low-threshold lasing [63], phase transition modification [39], chemical reactivity tuning [64, 65], Bose-Einstein condensation [66–68], and optical spin switching [69].

Figure 1**(b)** shows a schematic of the proposed waveguide-coupled resonator, where a bus waveguide is coupled to a closed resonant loop formed by two Sagnac interferometers. The closed resonant loop couples to the bus waveguide to form two directional couplers, and the interference between the waveguides connecting them is similar to that in a Mach-Zehnder interferometer (which is a finite impulse-response (FIR) filter). On the other hand, the interference between the closed resonant loop and the bus waveguide is similar to that in a ring resonator (which is an infinite impulse-response (IIR) filter). As a result, the device consists of both FIR and IIR filter elements. By introducing Sagnac interferometers in the resonant loop, such a device can also be regarded as a hybrid resonator consisting of both traveling-wave (formed by coherent interference between light waves in the closed-loop resonator and the

bus waveguide, similar to ring resonators) and standing-wave (formed by coherent interference induced by reflection between the two Sagnac interferometers, similar to Fabry-Perot cavities) resonator elements. The hybrid nature of the device in Fig. 1**(b)** allows for versatile coherent mode interference that can be tailored for spectral engineering of complex and demanding filtering functions.

The definitions of the device structural parameters are provided in **Table I**. In our following analysis, we investigate the spectral response of the device in Fig. 1**(b)** based on the scattering matrix method [33, 70], using the values of the transverse electric (TE) mode group index n_g = 4.3350 and the propagation loss factor α = 55 m^{-1} (i.e., 2.4 dB/cm) obtained from the fabricated silicon-on-insulator (SOI) devices in our previous work [70, 71]. The devices are designed for, but not limited to, the SOI platform — the principles outlined here are universal for all material platforms.

Table 1
Definitions of device structural parameters. SI: Sagnac interferometers.

Waveguides	**Physical length**	**Transmission factor** [a]	**Phase shift** [b]
Connecting waveguides between SI_1 and SI_2 (i = 1–3)	L_i	a_i	φ_i
Sagnac loop in SI_i (i = 1, 2)	L_{si}	a_{si}	φ_{si}
Directional couplers	Field transmission coefficient [c]	Field cross-coupling coefficient [c]	
Coupler in SI_i (i = 1, 2)	t_{si}	κ_{si}	
Coupler between SI_i and bus waveguide (i = 1, 2)	t_{bi}	κ_{bi}	

[a] $a_i = \exp(-\alpha L_i / 2)$, $a_{si} = \exp(-\alpha L_{si} / 2)$, where α is the power propagation loss factor.

[b] $\varphi_i = 2\pi n_g L_i / \lambda$, $\varphi_{si} = 2\pi n_g L_{si} / \lambda$, where n_g is the group index and λ is the wavelength.

[c] $t_{si}^2 + \kappa_{si}^2 = 1$ and $t_{bi}^2 + \kappa_{bi}^2 = 1$ for lossless coupling is assumed for all the directional couplers.

We tailor the spectral response of the device in Fig. 1**(b)** with bidirectional light propagation to realize optical analogues of Rabi splitting. The power transmission and reflection spectra with input from Port 1 are depicted in Fig. 1**(c)**. Unless elsewhere specified, the spectral response of the device is assumed to have an input from Port 1 in Fig. 1**(b)**, with the transmitted light at Port 2 and the reflected light back to Port 1. In Fig. 1**(c)**, the device structural parameters are t_{b1} = 0.98, t_{s1} = 0.87, t_{b2} = 0.90, t_{s2} = 0.71, L_{s1} = L_{s2} = 100 μm, and L_1 = L_2 = L_3 =100 μm. As can be seen, both the transmission spectra at Port 2 and the reflection spectra at Port 1 show Rabi-like splitting that features asymmetric split resonances, which result from coherent mode interference, analogous with the interaction between different quantum states

in multi-level atomic systems. Similar Rabi splitting spectra in the visible and mid-infrared regions have also been observed for PhC and plasmonic nanocavities [6, 39]. However, compared to these, the fabrication of waveguide-coupled resonators does not require high lithography resolution and shows higher tolerance to fabrication imperfections such as lithographic smoothing effects and quantization errors due to the finite grid size [70], which makes it much easier to accurately engineer the spectral response and overall device performance.

Iii. Anti-crossing Of Split Resonances

In this section, we investigate the resonance anti-crossing behavior of the device in Fig. 1(b), which is a key feature of Rabi splitting. A typical application of the anti-crossing behavior of the split resonances is to engineer the dispersion of the devices to generate artificial anomalous dispersion in devices that exhibit intrinsic normal dispersion [57, 58, 72], for applications to nonlinear optics. We also provide an analysis for the influence of the device structural parameters on the Rabi split resonances. To simplify the comparison, we vary only one structural parameter in each figure of this section, while keeping the others the same as in Fig. 1(c).

In Fig. 2 we compare the device spectral response for various ΔL_2, i.e., the variation in the length of L_2. As ΔL_2 changes, both the transmission spectra in Fig. 2(a-i) and the reflection spectra in Fig. 2(b-i) show obvious anti-crossing behavior in the split resonances when the two resonance modes approach each other. The center wavelengths and Q factors of the two resonance modes in Fig. 2(a-i) as functions of ΔL_2 are depicted in Figs. 2(a-ii) and 2(a-iii), respectively. The corresponding results for the two resonance modes in Fig. 2(b-i) are shown in Figs. 2(b-ii) and 2(b-iii). As can be seen, both the center wavelengths and the Q factors of the two split resonances show obvious changes with ΔL_2. This reflects the strong interaction between the two modes resulting from coherent mode interference, analogous to the coupling between the resonance and excitation states in Fig. 1(a) in the strong light-matter coupling regime.

Fig. 3 shows the device spectral response for various ΔL_3, i.e., the variation in the length of L_3. Similar to Fig. 2, the two Rabi split resonances avoid crossing each other in both the transmission (Fig. 3(a-i)) and reflection spectra (Fig. 3(b-i)). In both, the Q factors of the first resonance decreases with ΔL_3, while that of the second resonance increases with ΔL_3, showing the opposite trend to Figs. 2(a-iii) and (b-iii).

In Fig. 4, we compare the device spectral response for various ΔL_1, which is the length variation in L_1. In both the transmission and reflection spectra, the center wavelengths of the two split resonances remain almost unchanged, mainly because L_1 corresponds to the waveguide outside the closed resonant loop. In contrast, the Q factors of the two Rabi split resonances show obvious differences, with the Q factors of the first and second resonances decreasing and increasing with ΔL_1, respectively. This is similar to the trend for the changes of the Q factors with ΔL_3 in Figs. 3(a-iii) and (b-iii).

In practical applications, different values of ΔL_i (i = 1, 2, 3) in Figs. 2 – 4 can be achieved by varying the physical lengths of the corresponding waveguides in passive devices. By introducing thermo-optic micro-

heaters [32, 60] or PN junctions [73, 74] along the corresponding waveguides to tune their phase shifts, the changes of ΔL_i (i = 1, 2, 3) can also be realized via active tuning of passive devices, which allows for tunable Rabi splitting characteristics to meet the requirements of different applications.

In addition to phase shifts along the connecting waveguides, we investigate the influence of the coupling strengths of the directional couplers on the Rabi split resonances in Figs. 5 and 6. Since their influence on the center wavelengths of the split resonances is not as significant as varying ΔL_i (i = 1, 2, 3) in Figs. 2 – 4, we plot the spectra for different coupling strengths in the same figure to highlight the differences.

We first investigate the influence of the coupling strengths of the directional couplers in the two Sagnac interferometers (i.e., t_{s1} and t_{s2}), which determines the reflectivity of the Sagnac interferometers. Figure 5(a) shows the transmission and reflection spectra for various t_{s1}. As can be seen, the extinction ratios of the Rabi split resonances (defined as the difference between the maximum and minimum transmission) remain almost unchanged, while the spectral interval between the split resonances increases with t_{s1}. Similar trends are also observed in Fig. 5(b) that plot the transmission and reflection spectra versus t_{s2}. These result from the fact that changes in t_{s1} or t_{s2} alter the mutual coupling between the light waves propagating in two opposite directions, which varies the degree of Rabi mode splitting that have various spectral intervals between the split resonances.

In Fig. 6, we investigate the influence of varying the strengths of the directional couplers between the bus waveguide and Sagnac interferometers (i.e., t_{b1} and t_{b2}), i.e., the energy coupling strength between the closed resonant loop and bus waveguide. Figure 6(a) shows the transmission and reflection spectra versus t_{b1}, where the left resonance extinction ratio decreases with t_{b1}, while the right extinction ratio shows the opposite trend, reflecting their trade-off. The transmission and reflection spectra versus t_{b2} are shown in Fig. 6(b). Unlike the trade-off between the extinction ratios of the two resonances in Fig. 6(a), both resonance extinction ratios in Fig. 6(b) decrease with t_{b2}, highlighting the difference in the influence of t_{b1} and t_{b2} on the transmission and reflection spectra. Although t_{b1} and t_{b2} have more influence on the extinction ratios of the Rabi split resonances than t_{s1} and t_{s2}, their influence on the spectral interval between the split resonances is not as significant. This is mainly because the spectral interval between the split resonances, which reflects the degree of Rabi mode splitting, is determined by the coupling strength between the bidirectional light waves within the closed resonant loop. On the other hand, the extinction ratios of the split resonances are determined by the energy exchange between the resonant loop and the bus waveguide, which is similar to the different coupling regimes in ring resonators [75].

In practical applications, dynamic tuning of the coupling strength of the directional couplers in Figs. 5 and 6 can be realized by using Mach-Zehnder interferometric couplers to replace the directional couplers and adjusting the phase difference between the two arms. Recently, compact tunable directional couplers have also been demonstrated by directly integrating thermo-optic micro-heaters above the coupling regions [76, 77], which induces thermal gradients that lead to phase velocity mismatch between the coupled modes of the waveguides, enabling dynamic tuning of the coupling strength.

Iv. Transitions Between Lorentzian, Fano, And Rabi Splitting Spectral Lineshapes

The spectroscopic detection of radiation via physical processes such as scattering, absorption, or fluorescence has been widely used for characterizing the response of photon-matter systems, resulting in featured spectral lineshapes that unveil the fundamentals of light-matter interactions [1, 2]. In addition to Rabi splitting, there are other typical resonance spectral lineshapes. For example, the symmetric Lorentzian spectral lineshape, which describes the finite radiative lifetimes of excited states, and is commonly seen in the response spectra of ring resonators and Fabry-Perot cavities [71, 73, 78–80]. In addition, Fano resonances, which feature an asymmetric spectral lineshape induced by interference between a discrete quantum state and a continuum band of states [81, 82], have underpinned many applications such as switching [83], sensing [84, 85], lasing [86], and directional scattering [87, 88]. Despite originating from different underlying physics, the different spectral lineshapes are related to each other and sometimes can transit from one to another. In this section, we engineer the spectral response of the device in Fig. 1(b) to achieve transitions between Lorentzian, Fano, and Rabi splitting resonance spectral lineshapes.

Figure 7 shows the power transmission and reflection spectra for different values of L_3. The device structural parameters are L_{s1} = L_{s2} = 100 μm, L_1 = 200 μm, L_2 = 100 μm, t_{b1} = 0.83, t_{s1} = 0.707, t_{b2} = 0.98, and t_{s2} = 0.707. In Fig. 7, there is a single resonance with a symmetric Lorentzian spectral lineshape in both the transmission and reflection spectra when L_3 = 100 μm. As L_3 increases, the single resonance gradually splits to form a Fano asymmetric spectral lineshape in the reflection spectrum (when L_3 = 100.02 μm), and then evolves to become the Rabi splitting lineshape (when L_3 = 100.03 μm and 100.04 μm). By further increasing L_3, the split resonances gradually evolve to form a single symmetric Lorentzian spectral lineshape (when L_3 = 100.17 μm). This illustrates how transitions between the Lorentzian, Fano, and Rabi splitting resonance lineshapes can be realized by simply adjusting the phase shift along L_3. Another interesting phenomenon is that both Fano and Rabi splitting spectral lineshapes can be obtained for the same device with L_3 = 100.02 μm, where the Fano and Rabi splitting spectral lineshapes are achieved for the resonances observed in the reflection and transmission directions, respectively. Similarly, the transitions among the Lorentzian, Fano, and Rabi splitting resonance lineshapes can also be realized by changing L_2, as shown in Fig. 8.

The versatility and degree of control achieved using these advanced design techniques based on Sagnac interferometers [89–91] will likely have wide applications to many different areas beyond linear optical filters, including nonlinear optics and microcomb based devices [92–128] as well as quantum optical photonic chips [129–141] and photonic integrated chips based on novel 2D materials and structures [142–164].

V. Conclusions

We theoretically investigate optical analogues of Rabi splitting in integrated waveguide-coupled resonators formed by two Sagnac interferometers. Coherent mode interference in the proposed device is tailored to achieve optical analogues of Rabi splitting with a clear avoided behavior for the resonances. Moreover, transitions between the Lorentzian, Fano, and Rabi splitting resonance lineshapes are achieved by changing the phase shift along the connecting waveguide between the two Sagnac interferometers. A detailed analysis for the influence of the structural parameters on the device performance is also provided. Our work offers new possibilities for realizing optical analogues of Rabi splitting based on integrated waveguide-coupled resonators and provides new prospects for realizing optical analogues of quantum physics by exploiting Sagnac interference in integrated photonic devices. This will allow for attractive benefits in providing devices with compact footprint, high scalability, high fabrication tolerance, and mass producibility for practical applications.

Declarations

Competing Interests

The authors declare that there are no competing interests.

References

1. M. Ruggenthaler, N. Tancogne-Dejean, J. Flick, H. Appel, and A. Rubio, "From a quantum-electrodynamical light–matter description to novel spectroscopies," *Nature Reviews Chemistry,* vol. 2, no. 3, p. 0118, 2018/03/07 2018.
2. J. P. Reithmaier *et al.*, "Strong coupling in a single quantum dot–semiconductor microcavity system," *Nature,* vol. 432, no. 7014, pp. 197-200, 2004/11/01 2004.
3. K. Santhosh, O. Bitton, L. Chuntonov, and G. Haran, "Vacuum Rabi splitting in a plasmonic cavity at the single quantum emitter limit," *Nature Communications,* vol. 7, no. 1, p. ncomms11823, 2016/06/13 2016.
4. S. Nandi *et al.*, "Observation of Rabi dynamics with a short-wavelength free-electron laser," *Nature,* vol. 608, no. 7923, pp. 488-493, Aug 2022.
5. P. R. Berman, *Cavity quantum electrodynamics*. United States: Academic Press, 1994.
6. T. Yoshie *et al.*, "Vacuum Rabi splitting with a single quantum dot in a photonic crystal nanocavity," *Nature,* vol. 432, no. 7014, pp. 200-203, 2004/11/01 2004.
7. G. Khitrova, H. M. Gibbs, M. Kira, S. W. Koch, and A. Scherer, "Vacuum Rabi splitting in semiconductors," *Nature Physics,* vol. 2, no. 2, pp. 81-90, 2006/02/01 2006.
8. O. Bitton *et al.*, "Vacuum Rabi splitting of a dark plasmonic cavity mode revealed by fast electrons," *Nature Communications,* vol. 11, no. 1, p. 487, 2020/01/24 2020.
9. E. Peter *et al.*, "Exciton-Photon Strong-Coupling Regime for a Single Quantum Dot Embedded in a Microcavity," *Physical Review Letters,* vol. 95, no. 6, p. 067401, 08/01/ 2005.

10. K. Hennessy *et al.*, "Quantum nature of a strongly coupled single quantum dot–cavity system," *Nature,* vol. 445, no. 7130, pp. 896-899, 2007/02/01 2007.
11. J. Bellessa, C. Bonnand, J. C. Plenet, and J. Mugnier, "Strong Coupling between Surface Plasmons and Excitons in an Organic Semiconductor," *Physical Review Letters,* vol. 93, no. 3, p. 036404, 07/15/ 2004.
12. J. A. Hutchison, T. Schwartz, C. Genet, E. Devaux, and T. W. Ebbesen, "Modifying Chemical Landscapes by Coupling to Vacuum Fields," *Angewandte Chemie International Edition,* vol. 51, no. 7, pp. 1592-1596, 2012.
13. J. Feist, J. Galego, and F. J. Garcia-Vidal, "Polaritonic Chemistry with Organic Molecules," *ACS Photonics,* vol. 5, no. 1, pp. 205-216, 2018/01/17 2018.
14. F. P. Laussy, A. V. Kavokin, and I. A. Shelykh, "Exciton-Polariton Mediated Superconductivity," *Physical Review Letters,* vol. 104, no. 10, p. 106402, 03/09/ 2010.
15. E. Orgiu *et al.*, "Conductivity in organic semiconductors hybridized with the vacuum field," *Nature Materials,* vol. 14, no. 11, pp. 1123-1129, 2015/11/01 2015.
16. S. R. K. Rodriguez *et al.*, "Probing a Dissipative Phase Transition via Dynamical Optical Hysteresis," *Physical Review Letters,* vol. 118, no. 24, p. 247402, 06/16/ 2017.
17. M. Ramezani *et al.*, "Plasmon-exciton-polariton lasing," *Optica,* vol. 4, no. 1, pp. 31-37, 2017/01/20 2017.
18. R. Su *et al.*, "Room-Temperature Polariton Lasing in All-Inorganic Perovskite Nanoplatelets," *Nano Letters,* vol. 17, no. 6, pp. 3982-3988, 2017/06/14 2017.
19. A. Delteil, T. Fink, A. Schade, S. Höfling, C. Schneider, and A. İmamoğlu, "Towards polariton blockade of confined exciton–polaritons," *Nature Materials,* vol. 18, no. 3, pp. 219-222, 2019/03/01 2019.
20. G. Muñoz-Matutano *et al.*, "Emergence of quantum correlations from interacting fibre-cavity polaritons," *Nature Materials,* vol. 18, no. 3, pp. 213-218, 2019/03/01 2019.
21. D. M. Coles *et al.*, "Strong coupling between chlorosomes of photosynthetic bacteria and a confined optical cavity mode," *Nature Communications,* vol. 5, no. 1, p. 5561, 2014/11/28 2014.
22. J. D. Joannopoulos, P. R. Villeneuve, and S. Fan, "Photonic crystals: putting a new twist on light," *Nature,* vol. 386, no. 6621, pp. 143-149, 1997/03/01 1997.
23. T. Ozawa *et al.*, "Topological photonics," *Reviews of Modern Physics,* vol. 91, no. 1, p. 015006, 03/25/ 2019.
24. L. Lu, J. D. Joannopoulos, and M. Soljačić, "Topological photonics," *Nature Photonics,* vol. 8, no. 11, pp. 821-829, 2014/11/01 2014.
25. A. Regensburger, C. Bersch, M.-A. Miri, G. Onishchukov, D. N. Christodoulides, and U. Peschel, "Parity–time synthetic photonic lattices," *Nature,* vol. 488, no. 7410, pp. 167-171, 2012/08/01 2012.
26. Ş. K. Özdemir, S. Rotter, F. Nori, and L. Yang, "Parity–time symmetry and exceptional points in photonics," *Nature Materials,* vol. 18, no. 8, pp. 783-798, 2019/08/01 2019.

27. Z. Zou *et al.*, "Tunable two-stage self-coupled optical waveguide resonators," *Optics Letters,* vol. 38, no. 8, pp. 1215-1217, 2013/04/15 2013.
28. H. Tang, L. Zhou, J. Xie, L. Lu, and J. Chen, "Electromagnetically Induced Transparency in a Silicon Self-Coupled Optical Waveguide," *Journal of Lightwave Technology,* vol. 36, no. 11, pp. 2188-2195, 2018.
29. A. Li and W. Bogaerts, "Tunable electromagnetically induced transparency in integrated silicon photonics circuit," *Optics Express,* vol. 25, no. 25, pp. 31688-31695, 2017/12/11 2017.
30. H. Du *et al.*, "Ultra-sharp asymmetric Fano-like resonance spectrum on Si photonic platform," *Optics Express,* vol. 27, no. 5, pp. 7365-7372, 2019/03/04 2019.
31. A. Li and W. Bogaerts, "An actively controlled silicon ring resonator with a fully tunable Fano resonance," *APL Photonics,* vol. 2, no. 9, p. 096101, 2017.
32. T. Zhao *et al.*, "Independently tunable double Fano resonances based on waveguide-coupled cavities," *Optics Letters,* vol. 44, no. 12, pp. 3154-3157, 2019/06/15 2019.
33. H. Arianfard, J. Wu, S. Juodkazis, and D. J. Moss, "Advanced Multi-Functional Integrated Photonic Filters Based on Coupled Sagnac Loop Reflectors," *Journal of Lightwave Technology,* vol. 39, no. 5, pp. 1400-1408, 2021/03/01 2021.
34. H. Arianfard, J. Wu, S. Juodkazis, and D. J. Moss, "Three Waveguide Coupled Sagnac Loop Reflectors for Advanced Spectral Engineering," *Journal of Lightwave Technology,* vol. 39, no. 11, pp. 3478-3487, 2021/06/01 2021.
35. H. Arianfard, J. Wu, S. Juodkazis, and D. J. Moss, "Spectral Shaping Based on Coupled Sagnac Loop Reflectors Formed by a Self-Coupled Wire Waveguide," *IEEE Photonics Technology Letters,* vol. 33, no. 13, pp. 680-683, 2021.
36. M. Zhang *et al.*, "Electronically programmable photonic molecule," *Nature Photonics,* vol. 13, no. 1, pp. 36-40, 2019/01/01 2019.
37. C. Cui, L. Zhang, and L. Fan, "Photonic analog of Mollow triplet with on-chip photon-pair generation in dressed modes," *Optics Letters,* vol. 46, no. 19, pp. 4753-4756, 2021/10/01 2021.
38. L. Liu *et al.*, "Plasmon-induced thermal tuning of few-exciton strong coupling in 2D atomic crystals," *Optica,* vol. 8, no. 11, p. 1416, 2021.
39. X. Han, K. Wang, X. Xing, M. Wang, and P. Lu, "Rabi Splitting in a Plasmonic Nanocavity Coupled to a WS2 Monolayer at Room Temperature," *ACS Photonics,* vol. 5, no. 10, pp. 3970-3976, 2018.
40. Z. Liu *et al.*, "Fano resonance Rabi splitting of surface plasmons," *Scientific Reports,* vol. 7, no. 1, p. 8010, 2017/08/14 2017.
41. B. Li *et al.*, "Large Rabi splitting obtained in Ag-WS₂ strong-coupling heterostructure with optical microcavity at room temperature," *Opto-Electronic Advances,* vol. 2, no. 5, pp. 190008-1-190008-9, 2019/05/14 2019.
42. W. Gao, X. Li, M. Bamba, and J. Kono, "Continuous transition between weak and ultrastrong coupling through exceptional points in carbon nanotube microcavity exciton–polaritons," *Nature Photonics,*

vol. 12, no. 6, pp. 362-367, 2018.

43. L. Feng, Z. J. Wong, R.-M. Ma, Y. Wang, and X. Zhang, "Single-mode laser by parity-time symmetry breaking," *Science,* vol. 346, no. 6212, pp. 972-975, 2014.
44. P. St-Jean *et al.*, "Lasing in topological edge states of a one-dimensionallattice," *Nature Photonics,* vol. 11, no. 10, pp. 651-656, 2017/10/01 2017.
45. A. H. Safavi-Naeini *et al.*, "Electromagnetically induced transparency and slow light with optomechanics," *Nature,* vol. 472, no. 7341, pp. 69-73, 2011/04/01 2011.
46. L. Fan, K. Y. Fong, M. Poot, and H. X. Tang, "Cascaded optical transparency in multimode-cavity optomechanical systems," *Nature Communications,* vol. 6, no. 1, p. 5850, 2015/01/14 2015.
47. M. F. Yanik, W. Suh, Z. Wang, and S. Fan, "Stopping light in a waveguide with an all-optical analog of electromagnetically induced transparency," *Phys Rev Lett,* vol. 93, no. 23, p. 233903, Dec 3 2004.
48. Y.-C. Liu, B.-B. Li, and Y.-F. Xiao, "Electromagnetically induced transparency in optical microcavities," *Nanophotonics,* vol. 6, no. 5, pp. 789-811, 2017.
49. J. B. Khurgin, "Optical buffers based on slow light in electromagnetically induced transparent media and coupled resonator structures: comparative analysis," *Journal of the Optical Society of America B,* vol. 22, no. 5, pp. 1062-1074, 2005/05/01 2005.
50. H. Hodaei *et al.*, "Enhanced sensitivity at higher-order exceptional points," *Nature,* vol. 548, no. 7666, pp. 187-191, 2017/08/01 2017.
51. W. Chen, Ş. Kaya Özdemir, G. Zhao, J. Wiersig, and L. Yang, "Exceptional points enhance sensing in an optical microcavity," *Nature,* vol. 548, no. 7666, pp. 192-196, 2017/08/01 2017.
52. S. Zhang, D. A. Genov, Y. Wang, M. Liu, and X. Zhang, "Plasmon-induced transparency in metamaterials," *Phys Rev Lett,* vol. 101, no. 4, p. 047401, Jul 25 2008.
53. N. Liu *et al.*, "Planar metamaterial analogue of electromagnetically induced transparency for plasmonic sensing," *Nano Lett,* vol. 10, no. 4, pp. 1103-7, Apr 14 2010.
54. J. Zhu *et al.*, "On-chip single nanoparticle detection and sizing by mode splitting in an ultrahigh-Q microresonator," *Nature Photonics,* vol. 4, no. 1, pp. 46-49, 2010/01/01 2009.
55. Q. Li, Z. Zhang, F. Liu, M. Qiu, and Y. Su, "Dense wavelength conversion and multicasting in a resonance-split silicon microring," *Applied Physics Letters,* vol. 93, no. 8, p. 081113, 2008.
56. M. C. M. M. Souza, L. A. M. Barea, F. Vallini, G. F. M. Rezende, G. S. Wiederhecker, and N. C. Frateschi, "Embedded coupled microrings with high-finesse and close-spaced resonances for optical signal processing," *Optics Express,* vol. 22, no. 9, pp. 10430-10438, 2014/05/05 2014.
57. S. Kim *et al.*, "Dispersion engineering and frequency comb generation in thin silicon nitride concentric microresonators," *Nature Communications,* vol. 8, no. 1, p. 372, 2017/08/29 2017.
58. X. Xue *et al.*, "Normal-dispersion microcombs enabled by controllable mode interactions," *Laser & Photonics Reviews,* vol. 9, no. 4, pp. L23-L28, 2015.
59. B. Bahari *et al.*, "Photonic quantum Hall effect and multiplexed light sources of large orbital angular momenta," *Nature Physics,* vol. 17, no. 6, pp. 700-703, 2021/06/01 2021.

60. J. Wu *et al.*, "On-Chip Tunable Second-Order Differential-Equation Solver Based on a Silicon Photonic Mode-Split Microresonator," *Journal of Lightwave Technology,* vol. 33, no. 17, pp. 3542-3549, 2015.
61. F. H. Alast, G. Li, and K. W. Cheah, "Rabi-like splitting from large area plasmonic microcavity," *AIP Advances,* vol. 7, no. 8, p. 085201, 2017.
62. S. Longhi, "Quantum-optical analogies using photonic structures," *Laser & Photonics Review,* vol. 3, no. 3, pp. 243-261, 2009.
63. S. Christopoulos *et al.*, "Room-Temperature Polariton Lasing in Semiconductor Microcavities," *Physical Review Letters,* vol. 98, no. 12, p. 126405, 03/21/ 2007.
64. J. Galego, F. J. Garcia-Vidal, and J. Feist, "Suppressing photochemical reactions with quantized light fields," *Nature Communications,* vol. 7, no. 1, p. 13841, 2016/12/12 2016.
65. X. Shi, K. Ueno, T. Oshikiri, Q. Sun, K. Sasaki, and H. Misawa, "Enhanced water splitting under modal strong coupling conditions," *Nature Nanotechnology,* vol. 13, no. 10, pp. 953-958, 2018/10/01 2018.
66. J. Kasprzak *et al.*, "Bose–Einstein condensation of exciton polaritons," *Nature,* vol. 443, no. 7110, pp. 409-414, 2006/09/01 2006.
67. J. D. Plumhof, T. Stöferle, L. Mai, U. Scherf, and R. F. Mahrt, "Room-temperature Bose–Einstein condensation of cavity exciton–polaritons in a polymer," *Nature Materials,* vol. 13, no. 3, pp. 247-252, 2014/03/01 2014.
68. H. Deng, H. Haug, and Y. Yamamoto, "Exciton-polariton Bose-Einstein condensation," *Reviews of Modern Physics,* vol. 82, no. 2, pp. 1489-1537, 05/12/ 2010.
69. A. Amo *et al.*, "Exciton–polariton spin switches," *Nature Photonics,* vol. 4, no. 6, pp. 361-366, 2010/06/01 2010.
70. J. Wu, T. Moein, X. Xu, and D. J. Moss, "Advanced photonic filters based on cascaded Sagnac loop reflector resonators in silicon-on-insulator nanowires," *APL Photonics,* vol. 3, no. 4, p. 046102, 2018.
71. J. Wu, T. Moein, X. Xu, G. Ren, A. Mitchell, and D. J. Moss, "Micro-ring resonator quality factor enhancement via an integrated Fabry-Perot cavity," *APL Photonics,* vol. 2, no. 5, p. 056103, 2017.
72. Ó. B. Helgason *et al.*, "Dissipative solitons in photonic molecules," *Nature Photonics,* vol. 15, no. 4, pp. 305-310, 2021.
73. X. Sun *et al.*, "Tunable silicon Fabry–Perot comb filters formed by Sagnac loop mirrors," *Optics Letters,* vol. 38, no. 4, pp. 567-569, 2013.
74. H. Du *et al.*, "A Si Optical Modulator Based on Fano-Like Resonance," *IEEE Photonics Technology Letters,* vol. 33, no. 21, pp. 1209-1212, 2021.
75. J. Wu *et al.*, "Nested Configuration of Silicon Microring Resonator With Multiple Coupling Regimes," *IEEE Photonics Technology Letters,* vol. 25, no. 6, pp. 580-583, 2013.
76. R. Ge, Y. Luo, S. Gao, Y. Han, L. Chen, and X. Cai, "Reconfigurable silicon bandpass filters based on cascaded Sagnac loop mirrors," *Optics Letters,* vol. 46, no. 3, pp. 580-583, 2021.
77. X. Zi, L. Wang, K. Chen, and K. S. Chiang, "Mode-Selective Switch Based on Thermo-Optic Asymmetric Directional Coupler," *IEEE Photonics Technology Letters,* vol. 30, no. 7, pp. 618-621, 2018.

78. X. Jiang *et al.*, "Wavelength and bandwidth-tunable silicon comb filter based on Sagnac loop mirrors with Mach-Zehnder interferometer couplers," *Optics express,* vol. 24, no. 3, pp. 2183-2188, 2016.
79. H. Arianfard, B. Khajeheian, and R. Ghayour, "Tunable band (pass and stop) filters based on plasmonic structures using Kerr-type nonlinear rectangular nanocavity," *Optical Engineering,* vol. 56, no. 12, p. 121902, 2016.
80. S. Zheng *et al.*, "Compact tunable photonic comb filter on a silicon platform," *Optics letters,* vol. 42, no. 14, pp. 2762-2765, 2017.
81. M. F. Limonov, M. V. Rybin, A. N. Poddubny, and Y. S. Kivshar, "Fano resonances in photonics," *Nature Photonics,* vol. 11, no. 9, pp. 543-554, 2017.
82. A. E. Miroshnichenko, S. Flach, and Y. S. Kivshar, "Fano resonances in nanoscale structures," *Reviews of Modern Physics,* vol. 82, no. 3, pp. 2257-2298, 08/11/ 2010.
83. L. Stern, M. Grajower, and U. Levy, "Fano resonances and all-optical switching in a resonantly coupled plasmonic–atomic system," *Nature Communications,* vol. 5, no. 1, p. 4865, 2014/09/08 2014.
84. F. Hao, Y. Sonnefraud, P. V. Dorpe, S. A. Maier, N. J. Halas, and P. Nordlander, "Symmetry Breaking in Plasmonic Nanocavities: Subradiant LSPR Sensing and a Tunable Fano Resonance," *Nano Letters,* vol. 8, no. 11, pp. 3983-3988, 2008/11/12 2008.
85. Y. Deng, G. Cao, H. Yang, G. Li, X. Chen, and W. Lu, "Tunable and high-sensitivity sensing based on Fano resonance with coupled plasmonic cavities," *Scientific Reports,* vol. 7, no. 1, p. 10639, 2017/09/06 2017.
86. Y. Yu, W. Xue, E. Semenova, K. Yvind, and J. Mork, "Demonstration of a self-pulsing photonic crystal Fano laser," *Nature Photonics,* vol. 11, no. 2, pp. 81-84, 2017/02/01 2017.
87. S. N. Sheikholeslami, A. García-Etxarri, and J. A. Dionne, "Controlling the Interplay of Electric and Magnetic Modes via Fano-like Plasmon Resonances," *Nano Letters,* vol. 11, no. 9, pp. 3927-3934, 2011/09/14 2011.
88. C. Yan, K.-Y. Yang, and O. J. F. Martin, "Fano-resonance-assisted metasurface for color routing," *Light: Science & Applications,* vol. 6, no. 7, pp. e17017-e17017, 2017/07/01 2017.
89. Hamed Arianfard, Saulius Juodkazis, David J. Moss, and Jiayang Wu, “Sagnac interference in integrated photonics”, Applied Physics Reviews vol. 10 (2023).
90. Hamed Arianfard, Jiayang Wu, Saulius Juodkazis, and David J. Moss, “Spectral shaping based on optical waveguides with advanced Sagnac loop reflectors”, Paper No. PW22O-OE201-20, SPIE-Opto, Integrated Optics: Devices, Materials, and Technologies XXVI, SPIE Photonics West, San Francisco CA January 22 - 27 (2022). doi: 10.1117/12.2607902
91. Hamed Arianfard, Jiayang Wu, Saulius Juodkazis and David J. Moss, “Advanced multi-functional integrated photonic filters based on coupled Sagnac loop reflectors”, Paper 11691-4, PW21O-OE203-44, Silicon Photonics XVI, SPIE Photonics West, San Francisco CA March 6-11 (2021). doi.org/10.1117/12.2584020
92. A. Pasquazi, et al., “Sub-picosecond phase-sensitive optical pulse characterization on a chip”, Nature Photonics, vol. 5, no. 10, pp. 618-623 (2011).

93. Bao, C., et al., Direct soliton generation in microresonators, Opt. Lett, 42, 2519 (2017).
94. M.Ferrera et al., “CMOS compatible integrated all-optical RF spectrum analyzer”, Optics Express, vol. 22, no. 18, 21488 - 21498 (2014).
95. M. Kues, et al., “Passively modelocked laser with an ultra-narrow spectral width”, Nature Photonics, vol. 11, no. 3, pp. 159, 2017.
96. L. Razzari, et al., “CMOS-compatible integrated optical hyper-parametric oscillator,” Nature Photonics, vol. 4, no. 1, pp. 41-45, 2010.
97. M. Ferrera, et al., “Low-power continuous-wave nonlinear optics in doped silica glass integrated waveguide structures,” Nature Photonics, vol. 2, no. 12, pp. 737-740, 2008.
98. D. Duchesne, M. Peccianti, M. R. E. Lamont, et al., “Supercontinuum generation in a high index doped silica glass spiral waveguide,” Optics Express, vol. 18, no, 2, pp. 923-930, 2010.
99. H Bao, L Olivieri, M Rowley, ST Chu, BE Little, R Morandotti, DJ Moss, ... “Turing patterns in a fiber laser with a nested microresonator: Robust and controllable microcomb generation”, Physical Review Research 2 (2), 023395 (2020).
100. M. Ferrera, et al., “On-chip CMOS-compatible all-optical integrator”, Nature Communications, vol. 1, Article 29, 2010.
101. A. Pasquazi, et al., “All-optical wavelength conversion in an integrated ring resonator,” Optics Express, vol. 18, no. 4, pp. 3858-3863, 2010.
102. A.Pasquazi, Y. Park, J. Azana, et al., “Efficient wavelength conversion and net parametric gain via Four Wave Mixing in a high index doped silica waveguide,” Optics Express, vol. 18, no. 8, pp. 7634-7641, 2010.
103. M. Peccianti, M. Ferrera, L. Razzari, et al., “Subpicosecond optical pulse compression via an integrated nonlinear chirper,” Optics Express, vol. 18, no. 8, pp. 7625-7633, 2010.
104. A.Pasquazi, et al., “Self-locked optical parametric oscillation in a CMOS compatible microring resonator: a route to robust optical frequency comb generation on a chip,” Optics Express, vol. 21, no. 11, pp. 13333-13341, 2013.
105. Pasquazi, A. et al. Micro-combs: a novel generation of optical sources. Physics Reports vol. 729, 1-81 (2018).
106. Moss, D. J. et al., “New CMOS-compatible platforms based on silicon nitride and Hydex for nonlinear optics”, Nature photonics vol. 7, 597 (2013).
107. H. Bao, et al., Laser cavity-soliton microcombs, Nature Photonics, vol. 13, no. 6, pp. 384-389, Jun. 2019.
108. A. Cutrona et al., “High Conversion Efficiency in Laser Cavity-Soliton Microcombs”, Optics Express Vol. 30, Issue 22, pp. 39816-39825 (2022). https://doi.org/10.1364/OE.470376.
109. M. Rowley et al., “Self-emergence of robust solitons in a micro-cavity”, Nature vol. 608 (7922) 303–309 (2022).

110. Xu, X., et al., Photonic microwave true time delays for phased array antennas using a 49 GHz FSR integrated micro-comb source, Photonics Research, vol. 6, B30-B36 (2018).
111. Xu, et al., “Advanced adaptive photonic RF filters with 80 taps based on an integrated optical micro-comb source,” Journal of Lightwave Technology, vol. 37, no. 4, pp. 1288-1295 (2019).
112. X. Xu, et al., Broadband microwave frequency conversion based on an integrated optical micro-comb source”, Journal of Lightwave Technology, vol. 38 no. 2, pp. 332-338, 2020.
113. M. Tan, et al., “Photonic RF and microwave filters based on 49GHz and 200GHz Kerr microcombs”, Optics Comm. vol. 465,125563, Feb. 22. 2020.
114. X. Xu, et al., “Photonic RF and microwave integrator with soliton crystal microcombs”, IEEE Transactions on Circuits and Systems II: Express Briefs, vol. 67, no. 12, pp. 3582-3586, 2020. DOI:10.1109/TCSII.2020.2995682.
115. X. Xu, et al., “High performance RF filters via bandwidth scaling with Kerr micro-combs,” APL Photonics, vol. 4 (2) 026102. 2019.
116. M. Tan, et al., “Microwave and RF photonic fractional Hilbert transformer based on a 50 GHz Kerr micro-comb”, Journal of Lightwave Technology, vol. 37, no. 24, pp. 6097 – 6104, 2019.
117. M. Tan, et al., “RF and microwave fractional differentiator based on photonics”, IEEE Transactions on Circuits and Systems: Express Briefs, vol. 67, no.11, pp. 2767-2771, 2020. DOI:10.1109/TCSII.2020.2965158.
118. M. Tan, X. Xu, J. Wu, R. Morandotti, A. Mitchell, and D. J. Moss, “RF and microwave high bandwidth signal processing based on Kerr Micro-combs”, Advances in Physics X, VOL. 6, NO. 1, 1838946 (2021). DOI:10.1080/23746149.2020.1838946.
119. X. Xu, et al., “Advanced RF and microwave functions based on an integrated optical frequency comb source,” Opt. Express, vol. 26 (3) 2569 (2018).
120. M. Tan, X. Xu, J. Wu, B. Corcoran, A. Boes, T. G. Nguyen, S. T. Chu, B. E. Little, R.Morandotti, A. Lowery, A. Mitchell, and D. J. Moss, “"Highly Versatile Broadband RF Photonic Fractional Hilbert Transformer Based on a Kerr Soliton Crystal Microcomb”, Journal of Lightwave Technology vol. 39 (24) 7581-7587 (2021).
121. Wu, J. et al. RF Photonics: An Optical Microcombs’ Perspective. IEEE Journal of Selected Topics in Quantum Electronics Vol. 24, 6101020, 1-20 (2018).
122. T. G. Nguyen et al., “Integrated frequency comb source-based Hilbert transformer for wideband microwave photonic phase analysis,” Opt. Express, vol. 23, no. 17, pp. 22087-22097, Aug. 2015.
123. X. Xu, J. Wu, M. Shoeiby, T. G. Nguyen, S. T. Chu, B. E. Little, R. Morandotti, A. Mitchell, and D. J. Moss, “Reconfigurable broadband microwave photonic intensity differentiator based on an integrated optical frequency comb source,” APL Photonics, vol. 2, no. 9, 096104, Sep. 2017.
124. B. Corcoran, et al., “Ultra-dense optical data transmission over standard fiber with a single chip source”, Nature Communications, vol. 11, Article:2568, 2020.

125. X. Xu, et al., “11 TOPs photonic convolutional accelerator for optical neural networks”, Nature vol. 589, 44-51 (2021).
126. Mengxi Tan, Xingyuan Xu, Jiayang Wu, Roberto Morandotti, Arnan Mitchell, and David J. Moss, “Neuromorphic computing based on wavelength-division multiplexing”, vol. 28 Early Access IEEE Journal of Selected Topics in Quantum Electronics. DOI:10.1109/JSTQE.2022.3203159.
127. Yang Sun, Jiayang Wu, Mengxi Tan, Xingyuan Xu, Yang Li, Roberto Morandotti, Arnan Mitchell, and David Moss, “Applications of optical micro-combs”, Advances in Optics and Photonics (2023). DOI:10.1364/AOP.470264.
128. Yunping Bai, Xingyuan Xu,1, Mengxi Tan, Yang Sun, Yang Li, Jiayang Wu, Roberto Morandotti, Arnan Mitchell, Kun Xu, and David J. Moss, “Photonic multiplexing techniques for neuromorphic computing”, accepted with modest revisions, Nanophotonics vol. 12 (2023). DOI:10.1515/nanoph-2022-0485.
129. Kues, M. et al. “Quantum optical microcombs”, Nature Photonics 13, (3) 170-179 (2019). doi:10.1038/s41566-019-0363-0
130. C.Reimer, L. Caspani, M. Clerici, et al., “Integrated frequency comb source of heralded single photons,” Optics Express, vol. 22, no. 6, pp. 6535-6546, 2014.
131. C.Reimer, et al., “Cross-polarized photon-pair generation and bi-chromatically pumped optical parametric oscillation on a chip”, Nature Communications, vol. 6, Article 8236, 2015. DOI: 10.1038/ncomms9236.
132. L. Caspani, C. Reimer, M. Kues, et al., “Multifrequency sources of quantum correlated photon pairs on-chip: a path toward integrated Quantum Frequency Combs,” Nanophotonics, vol. 5, no. 2, pp. 351-362, 2016.
133. C. Reimer et al., “Generation of multiphoton entangled quantum states by means of integrated frequency combs,” Science, vol. 351, no. 6278, pp. 1176-1180, 2016.
134. M. Kues, et al., “On-chip generation of high-dimensional entangled quantum states and their coherent control”, Nature, vol. 546, no. 7660, pp. 622-626, 2017.
135. P. Roztocki et al., “Practical system for the generation of pulsed quantum frequency combs,” Optics Express, vol. 25, no. 16, pp. 18940-18949, 2017.
136. Y. Zhang, et al., “Induced photon correlations through superposition of two four-wave mixing processes in integrated cavities”, Laser and Photonics Reviews, vol. 14, no. 7, pp. 2000128, 2020. DOI: 10.1002/lpor.202000128
137. C. Reimer, et al., “High-dimensional one-way quantum processing implemented on d-level cluster states”, Nature Physics, vol. 15, no.2, pp. 148–153, 2019.
138. P.Roztocki et al., “Complex quantum state generation and coherent control based on integrated frequency combs”, Journal of Lightwave Technology vol. 37 (2) 338-347 (2019).
139. S. Sciara et al., “Generation and Processing of Complex Photon States with Quantum Frequency Combs”, IEEE Photonics Technology Letters 31 (23) 1862-1865 (2019). DOI: 10.1109/LPT.2019.2944564.

140. Stefania Sciara, Piotr Roztocki, Bennet Fisher, Christian Reimer, Luis Romero Cortez, William J. Munro, David J. Moss, Alfonso C. Cino, Lucia Caspani, Michael Kues, J. Azana, and Roberto Morandotti, “Scalable and effective multilevel entangled photon states: A promising tool to boost quantum technologies”, Nanophotonics vol. 10 (18), 4447–4465 (2021). DOI:10.1515/nanoph-2021-0510.
141. L. Caspani, C. Reimer, M. Kues, et al., “Multifrequency sources of quantum correlated photon pairs on-chip: a path toward integrated Quantum Frequency Combs,” Nanophotonics, vol. 5, no. 2, pp. 351-362, 2016.
142. Yuning Zhang, Jiayang Wu, Yang Qu, Yunyi Yang, Linnan Jia, Baohua Jia, and David J. Moss, “Enhanced supercontinuum generated in SiN waveguides coated with GO films”, Advanced Materials Technologies vol. 8 (2023). DOI: 10.1002/admt.202201796.
143. Yuning Zhang, Jiayang Wu, Linnan Jia, Yang Qu, Baohua Jia, and David J. Moss, “Graphene oxide for
144. Jiayang Wu, H.Lin, D. J. Moss, T.K. Loh, Baohua Jia, “Graphene oxide: new opportunities for electronics, photonics, and optoelectronics”, Nature Reviews Chemistry vol. 7 (2023). DOI:10.1038/s41570-022-00458-7.
145. Yang Qu, Jiayang Wu, Yuning Zhang, Yunyi Yang, Linnan Jia, Baohua Jia, and David J. Moss, “Photo thermal tuning in GO-coated integrated waveguides”, Micromachines vol. 13 1194 (2022). doi.org/10.3390/mi13081194
146. Yuning Zhang, Jiayang Wu, Yunyi Yang, Yang Qu, Houssein El Dirani, Romain Crochemore, Corrado Sciancalepore, Pierre Demongodin, Christian Grillet, Christelle Monat, Baohua Jia, and David J. Moss, “Enhanced self-phase modulation in silicon nitride waveguides integrated with 2D graphene oxide films”, IEEE Journal of Selected Topics in Quantum Electronics vol. 28 Early Access (2022). DOI: 10.1109/JSTQE.2022.3177385
147. Yuning Zhang, Jiayang Wu, Yunyi Yang, Yang Qu, Linnan Jia, Baohua Jia, and David J. Moss, “Enhanced spectral broadening of femtosecond optical pulses in silicon nanowires integrated with 2D graphene oxide films”, Micromachines vol. 13 756 (2022). DOI:10.3390/mi13050756.
148. Linnan Jia, Jiayang Wu, Yuning Zhang, Yang Qu, Baohua Jia, Zhigang Chen, and David J. Moss, “Fabrication Technologies for the On-Chip Integration of 2D Materials”, Small: Methods vol. 6, 2101435 (2022). DOI:10.1002/smtd.202101435.
149. Yuning Zhang, Jiayang Wu, Yang Qu, Linnan Jia, Baohua Jia, and David J. Moss, “Design and optimization of four-wave mixing in microring resonators integrated with 2D graphene oxide films”, Journal of Lightwave Technology vol. 39 (20) 6553-6562 (2021). DOI:10.1109/JLT.2021.3101292.
150. Yuning Zhang, Jiayang Wu, Yang Qu, Linnan Jia, Baohua Jia, and David J. Moss, “Optimizing the Kerr nonlinear optical performance of silicon waveguides integrated with 2D graphene oxide films”, Journal of Lightwave Technology vol. 39 (14) 4671-4683 (2021). DOI: 10.1109/JLT.2021.3069733.
151. Yang Qu, Jiayang Wu, Yuning Zhang, Yao Liang, Baohua Jia, and David J. Moss, “Analysis of four-wave mixing in silicon nitride waveguides integrated with 2D layered graphene oxide films”, Journal

of Lightwave Technology vol. 39 (9) 2902-2910 (2021). DOI: 10.1109/JLT.2021.3059721.

152. Jiayang Wu, Linnan Jia, Yuning Zhang, Yang Qu, Baohua Jia, and David J. Moss,“ Graphene oxide: versatile films for flat optics to nonlinear photonic chips”, Advanced Materials 33 (3) 2006415, pp.1-29 (2021). DOI:10.1002/adma.202006415.
153. Y. Qu, J. Wu, Y. Zhang, L. Jia, Y. Yang, X. Xu, S. T. Chu, B. E. Little, R. Morandotti, B. Jia, and D. J. Moss, “Graphene oxide for enhanced optical nonlinear performance in CMOS compatible integrated devices”, Paper No. 11688-30, PW21O-OE109-36, 2D Photonic Materials and Devices IV, SPIE Photonics West, San Francisco CA March 6-11 (2021). doi.org/10.1117/12.2583978
154. Yang Qu, Jiayang Wu, Yunyi Yang, Yuning Zhang, Yao Liang, Houssein El Dirani, Romain Crochemore, Pierre Demongodin, Corrado Sciancalepore, Christian Grillet, Christelle Monat, Baohua Jia, and David J. Moss, “Enhanced nonlinear four-wave mixing in silicon nitride waveguides integrated with 2D layered graphene oxide films”, Advanced Optical Materials vol. 8 (21) 2001048 (2020). DOI: 10.1002/adom.202001048. arXiv:2006.14944.
155. Yuning Zhang, Yang Qu, Jiayang Wu, Linnan Jia, Yunyi Yang, Xingyuan Xu, Baohua Jia, and David J. Moss, “Enhanced Kerr nonlinearity and nonlinear figure of merit in silicon nanowires integrated with 2D graphene oxide films”, ACS Applied Materials and Interfaces vol. 12 (29) 33094–33103 June 29 (2020). DOI:10.1021/acsami.0c07852
156. Jiayang Wu, Yunyi Yang, Yang Qu, Yuning Zhang, Linnan Jia, Xingyuan Xu, Sai T. Chu, Brent E. Little, Roberto Morandotti, Baohua Jia,* and David J. Moss*, “Enhanced nonlinear four-wave mixing in microring resonators integrated with layered graphene oxide films”, Small vol. 16 (16) 1906563 April 23 (2020). DOI: 10.1002/smll.201906563
157. Jiayang Wu, Yunyi Yang, Yang Qu, Xingyuan Xu, Yao Liang, Sai T. Chu, Brent E. Little, Roberto Morandotti, Baohua Jia, and David J. Moss, “Graphene oxide waveguide polarizers and polarization selective micro-ring resonators”, Paper 11282-29, SPIE Photonics West, San Francisco, CA, 4 - 7 February (2020). doi: 10.1117/12.2544584
158. Jiayang Wu, Yunyi Yang, Yang Qu, Xingyuan Xu, Yao Liang, Sai T. Chu, Brent E. Little, Roberto Morandotti, Baohua Jia, and David J. Moss, “Graphene oxide waveguide polarizers and polarization selective micro-ring resonators”, Laser and Photonics Reviews vol. 13 (9) 1900056 (2019). DOI:10.1002/lpor.201900056.
159. Yunyi Yang, Jiayang Wu, Xingyuan Xu, Sai T. Chu, Brent E. Little, Roberto Morandotti, Baohua Jia, and David J. Moss, “Enhanced four-wave mixing in graphene oxide coated waveguides”, Applied Physics Letters Photonics vol. 3 120803 (2018). doi: 10.1063/1.5045509.
160. E.D Ghahramani, DJ Moss, JE Sipe, “Full-band-structure calculation of first-, second-, and third-harmonic optical response coefficients of ZnSe, ZnTe, and CdTe”, Physical Review B 43 (12), 9700 (1991).
161. C Grillet, C Smith, D Freeman, S Madden, B Luther-Davies, EC Magi, ... “Efficient coupling to chalcogenide glass photonic crystal waveguides via silica optical fiber nanowires”, Optics Express vol. 14 (3), 1070-1078 (2006).

162. S Tomljenovic-Hanic, MJ Steel, CM de Sterke, DJ Moss, “High-Q cavities in photosensitive photonic crystals” Optics Letters vol. 32 (5), 542-544 (2007).

163. Linnan Jia, Dandan Cui, Jiayang Wu, Haifeng Feng, Tieshan Yang, Yunyi Yang, Yi Du, Weichang Hao, Baohua Jia, David J. Moss, “BiOBr nanoflakes with strong nonlinear optical properties towards hybrid integrated photonic devices”, Applied Physics Letters Photonics vol. 4 090802 (2019). DOI: 10.1063/1.5116621

164. Linnan Jia, Jiayang Wu, Yunyi Yang, Yi Du, Baohua Jia, David J. Moss, “Large Third-Order Optical Kerr Nonlinearity in Nanometer-Thick PdSe2 2D Dichalcogenide Films: Implications for Nonlinear Photonic Devices”, ACS Applied Nano Materials vol. 3 (7) 6876–6883 (2020).

Figures

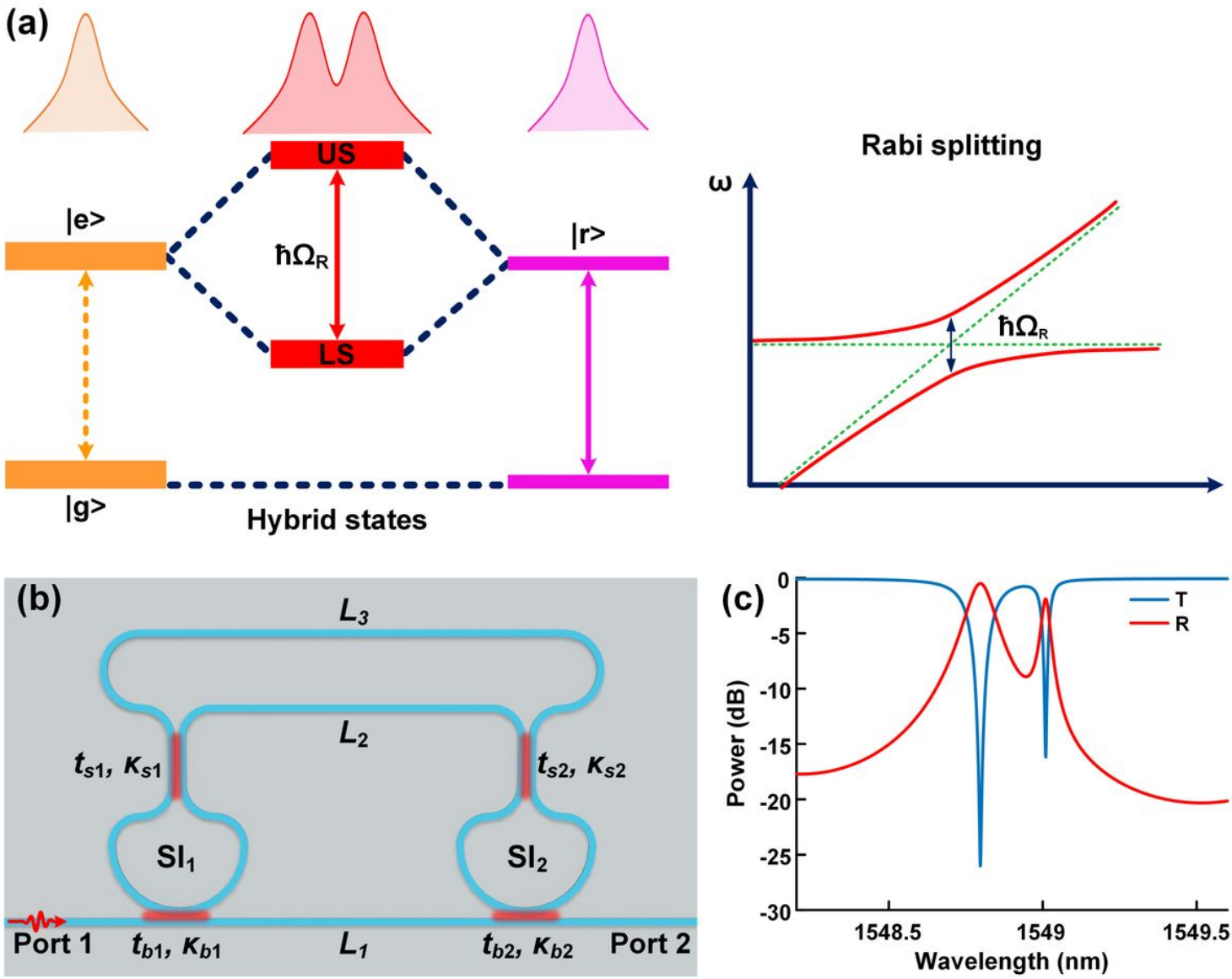

Figure 1

(a) Schematic illustration of Rabi splitting. |e⟩: matter excitation state. |r⟩: resonance state. |g⟩: ground state. US: upper state. UL: lower state. $\hbar\Omega_R$: Rabi splitting energy, with $\hbar$ denoting the Planck constant and Ω_R the frequency separation. (b) Schematic configuration of a waveguide-coupled resonator consisting of a bus waveguide side coupled to a resonant loop formed by two Sagnac interferometers. The definitions of t_{bi} (i = 1, 2), κ_{bi} (i = 1, 2), t_{si} (i = 1, 2), κ_{si} (i = 1, 2), L_{si} (i = 1, 2), and L_i (i = 1–3) are provided in Table I. (c) Power transmission and reflection spectra with input from Port 1 in (b). T: Transmission spectrum at Port 2. R: reflection spectrum at Port 1. The structural parameters are t_{b1} = 0.98, t_{s1} = 0.87, t_{b2} = 0.90, t_{s2} = 0.71, L_{s1} = L_{s2} = 100 μm, and L_1 = L_2 = L_3 =100 μm.

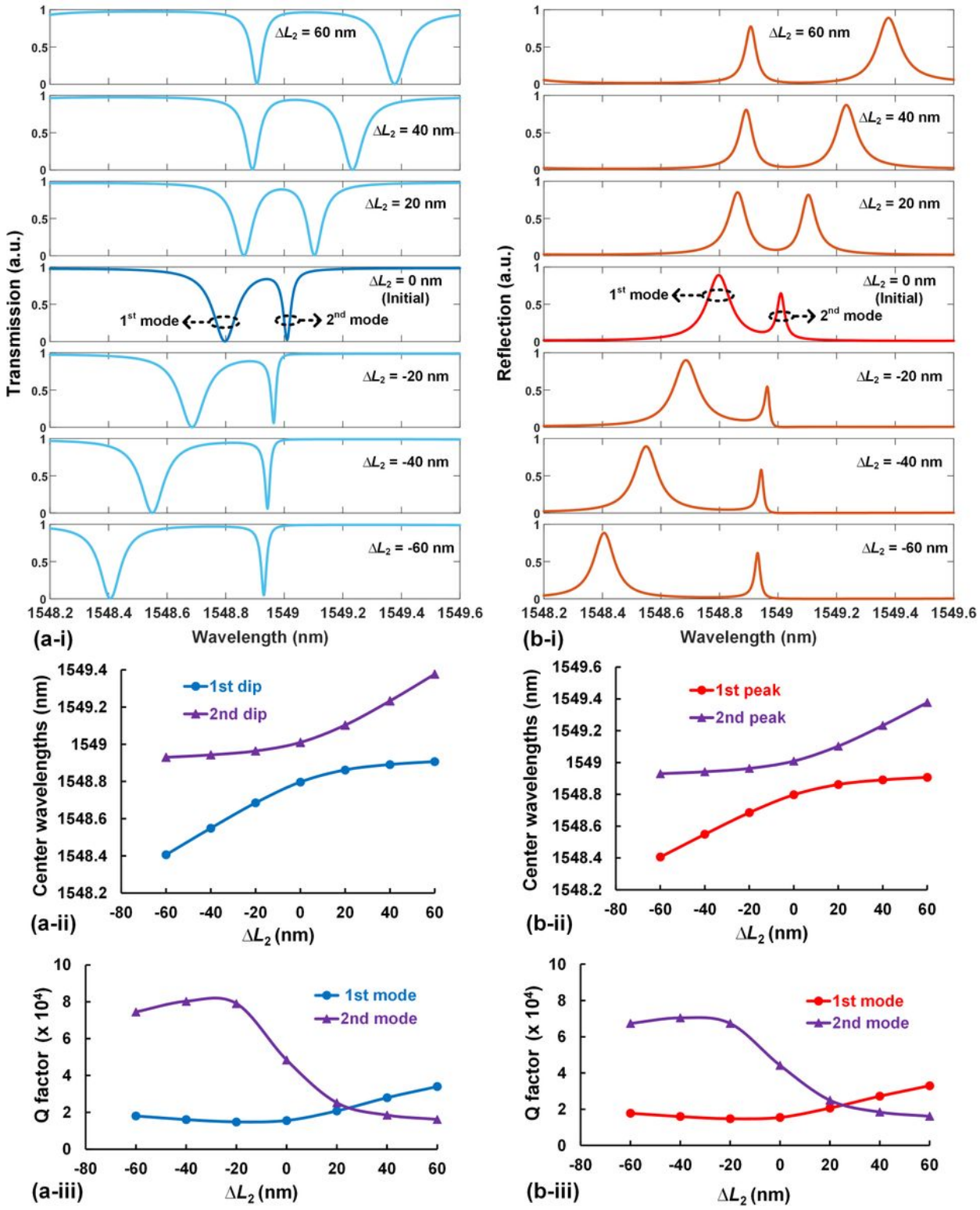

Figure 2

Influence of the variation in the length of L_2 (ΔL_2) on the device spectral response. (a) Rabi split resonances for various ΔL_2 at the transmission port. (b) Rabi split resonances for various ΔL_2 at the reflection port. In (a) and (b), (i) shows the power transmission spectra, (ii) shows the center wavelengths of the two resonances in (i) as functions of ΔL_2, and (iii) shows the Q factors of the two resonances in (i)

as functions of ΔL_2. The structural parameters are kept the same as those in Fig. 1(c) except for the variation in the length of L_2.

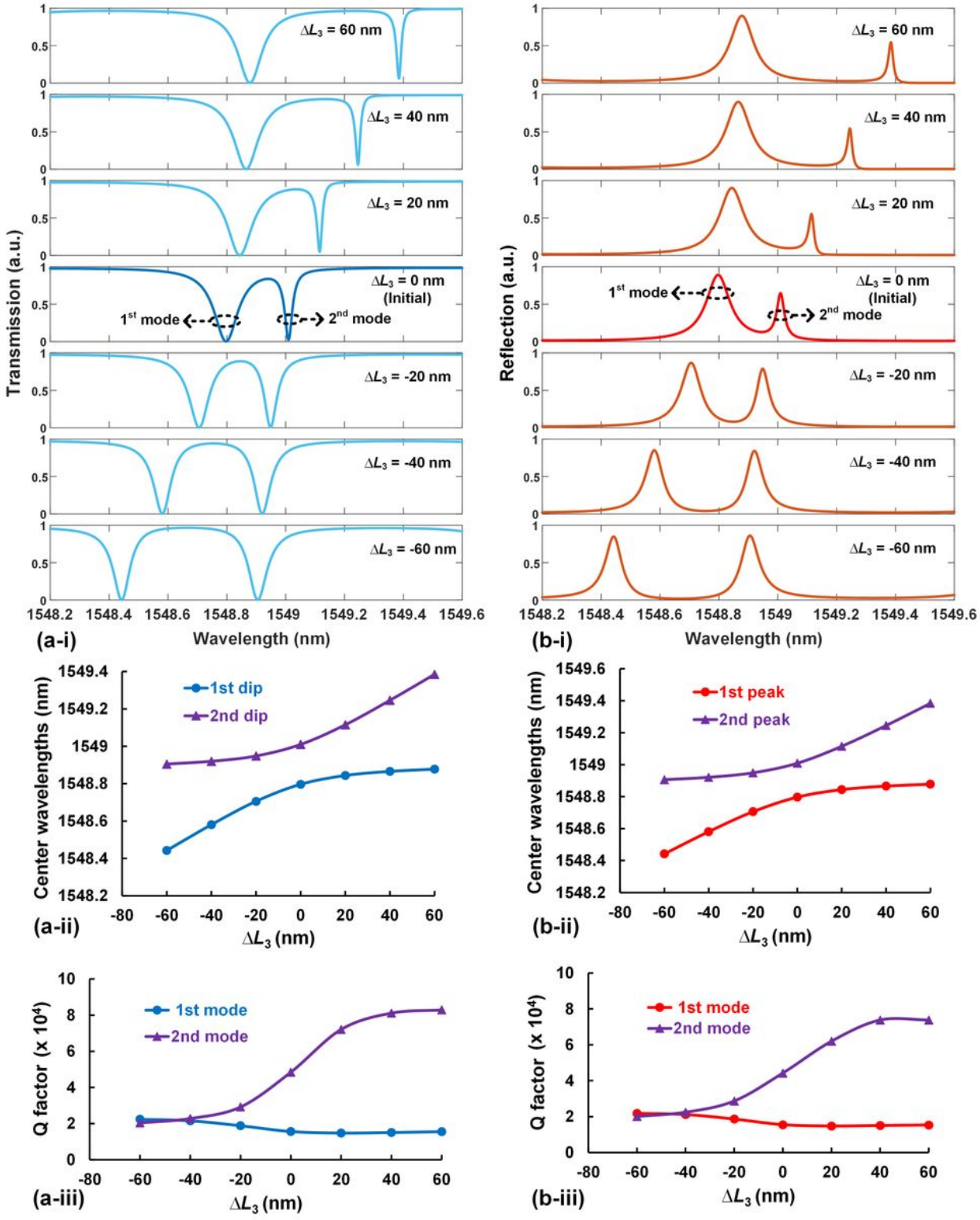

Figure 3

Influence of the variation in the length of L_3 (ΔL_3) on the device spectral response. (a) Rabi split resonances for various ΔL_3 at the transmission port. (b) Rabi split resonances for various ΔL_3 at the

reflection port. In (a) and (b), (i) shows the power transmission spectra, (ii) shows the center wavelengths of the two resonances in (i) as functions of ΔL_3, and (iii) shows the Q factors of the two resonances in (i) as functions of ΔL_3. The structural parameters are kept the same as those in Fig. 1(c) except for the variation in the length of L_3.

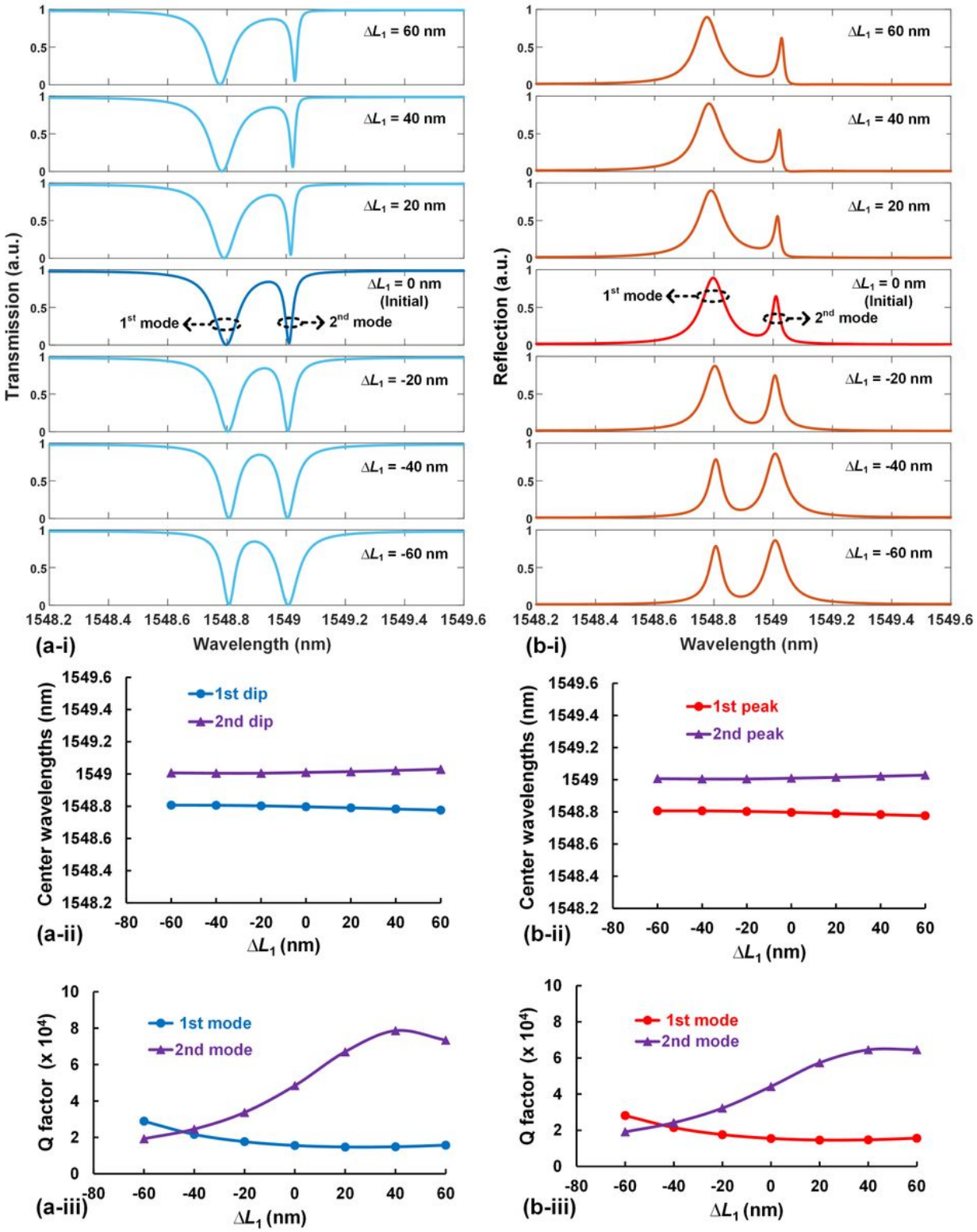

Figure 4

Influence of the variation in the length of L_1 (ΔL_1) on the device spectral response. (a) Rabi split resonances for various ΔL_1 at the transmission port. (b) Rabi split resonances for various ΔL_1 at the reflection port. In (a) and (b), (i) shows the power transmission spectra, (ii) shows the center wavelengths of the two resonances in (i) as functions of ΔL_1, and (iii) shows the Q factors of the two resonances in (i) as functions of ΔL_1. The structural parameters are kept the same as those in Fig. 1(c) except for the variation in the length of L_1.

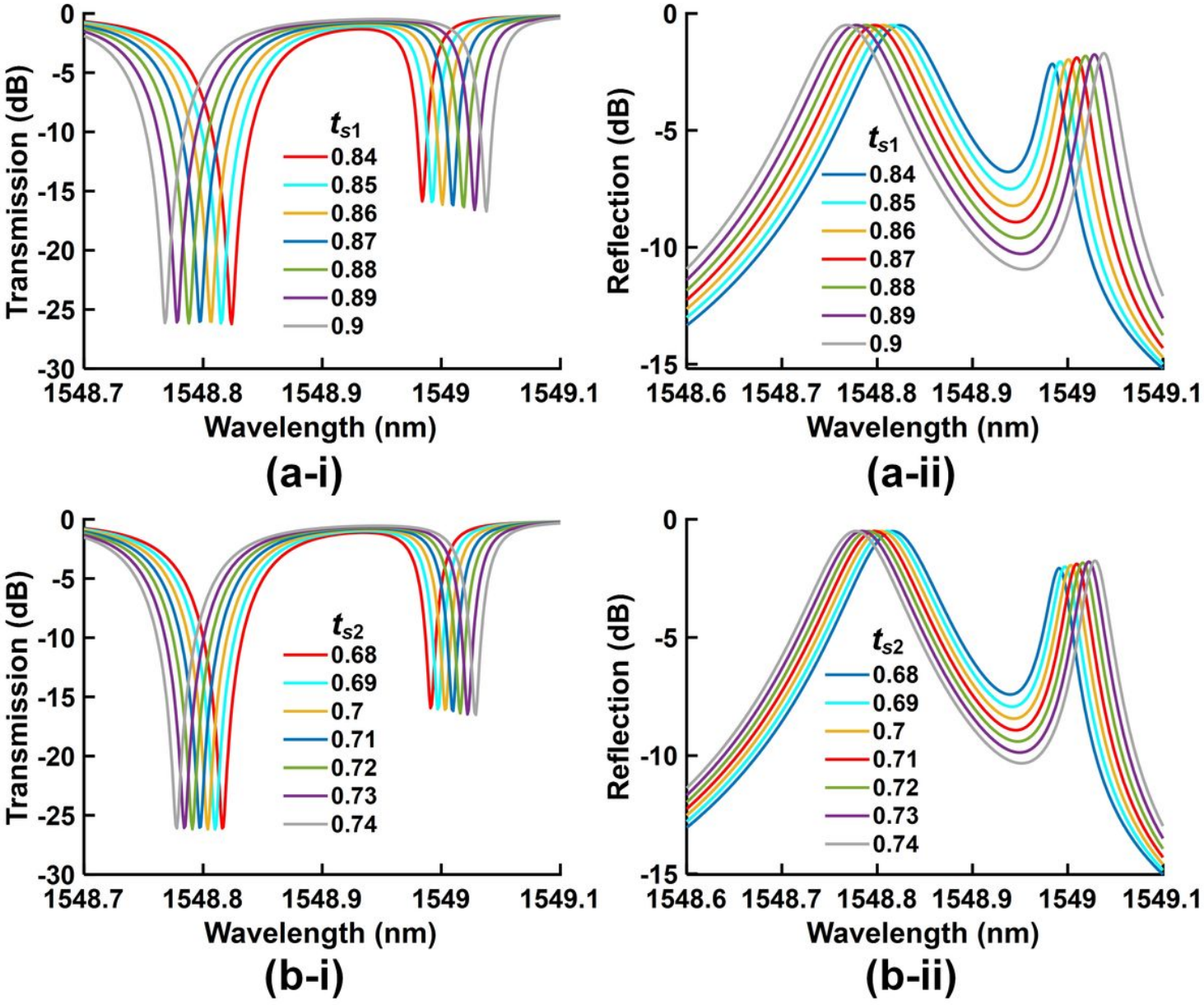

Figure 5

(a) Influence of t_{s1} on Rabi split resonances at (i) the transmission port and (ii) the reflection port. (b) Influence of t_{s2} on Rabi split resonances at (i) the transmission port and (ii) the reflection port. In (a) and (b), the structural parameters are kept the same as those in Fig. 1(c) except for t_{s1} and t_{s2}, respectively.

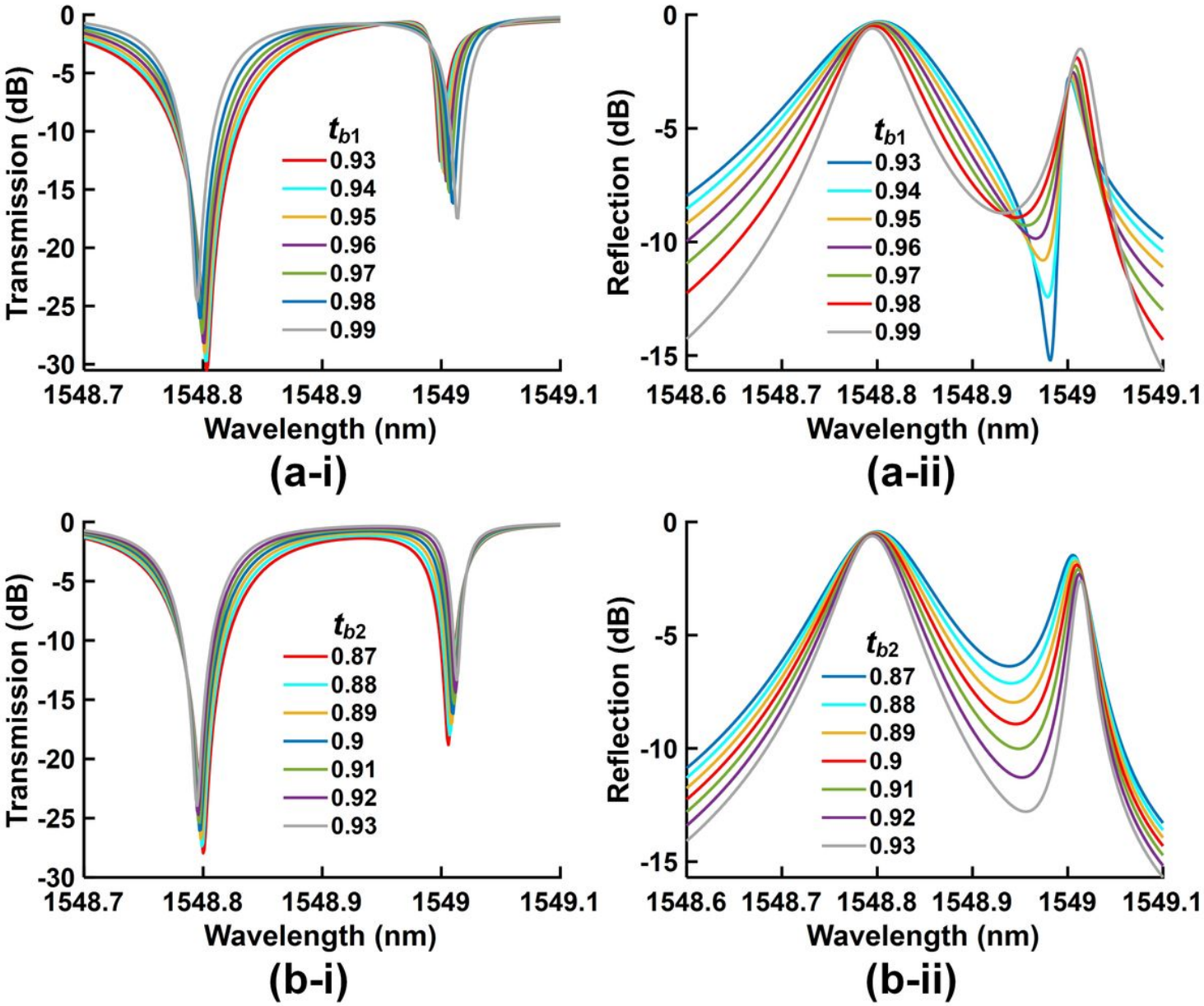

Figure 6

(a) Influence of t_{b1} on Rabi split resonances at (i) the transmission port and (ii) the reflection port. (b) Influence of t_{b2} on Rabi split resonances at (i) the transmission port and (ii) the reflection port. In (a) and (b), the structural parameters are kept the same as those in Fig. 1(c) except for t_{b1} and t_{b2}, respectively.

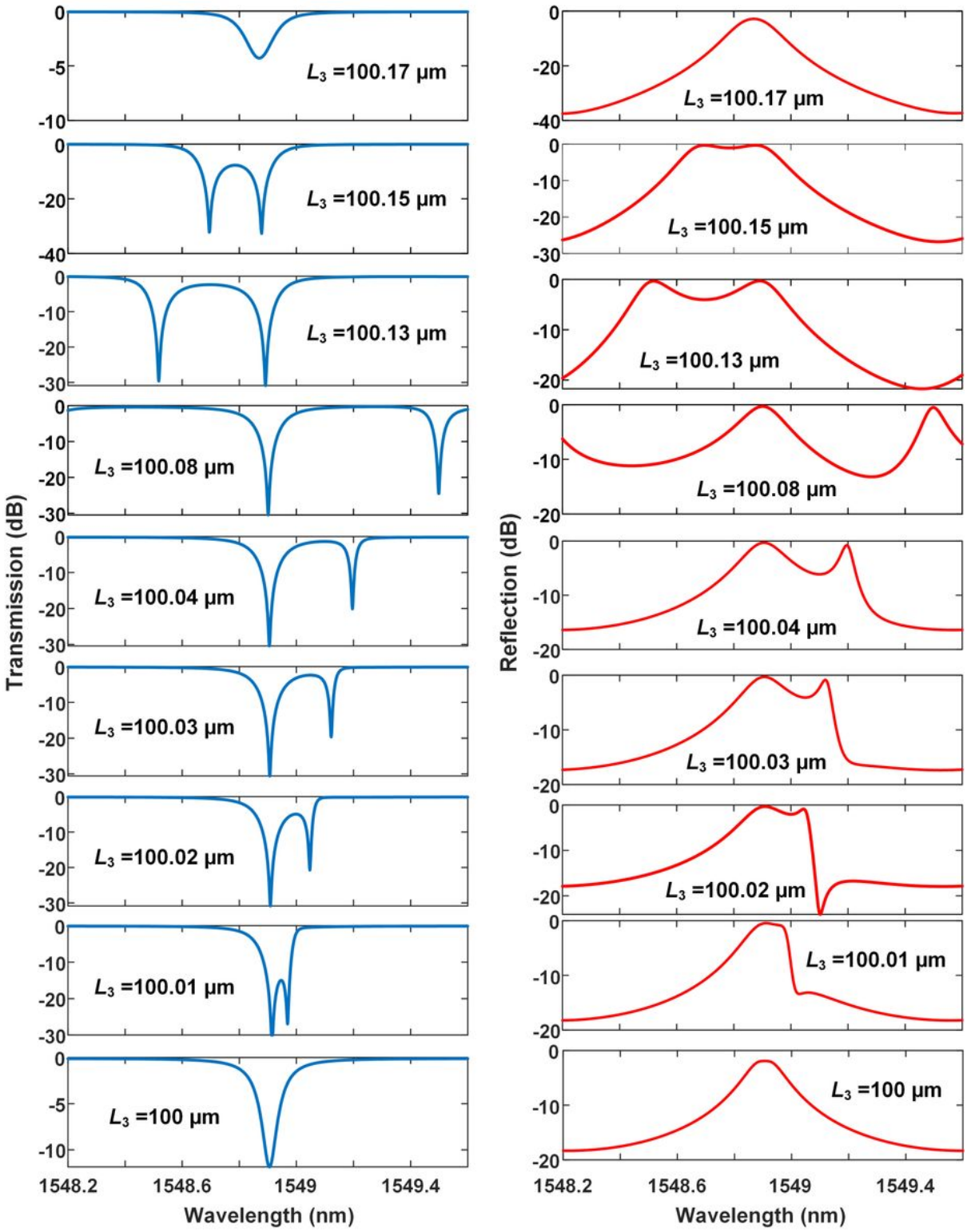

Figure 7

Power transmission (left) and reflection (right) spectra for various L_3. The structural parameters are t_{b1} = 0.83, t_{s1} = 0.707, t_{b2} = 0.98, t_{s2} = 0.707, L_{s1} = L_{s2} = 100 μm, L_1 = 200 μm, and L_2 = 100 μm.

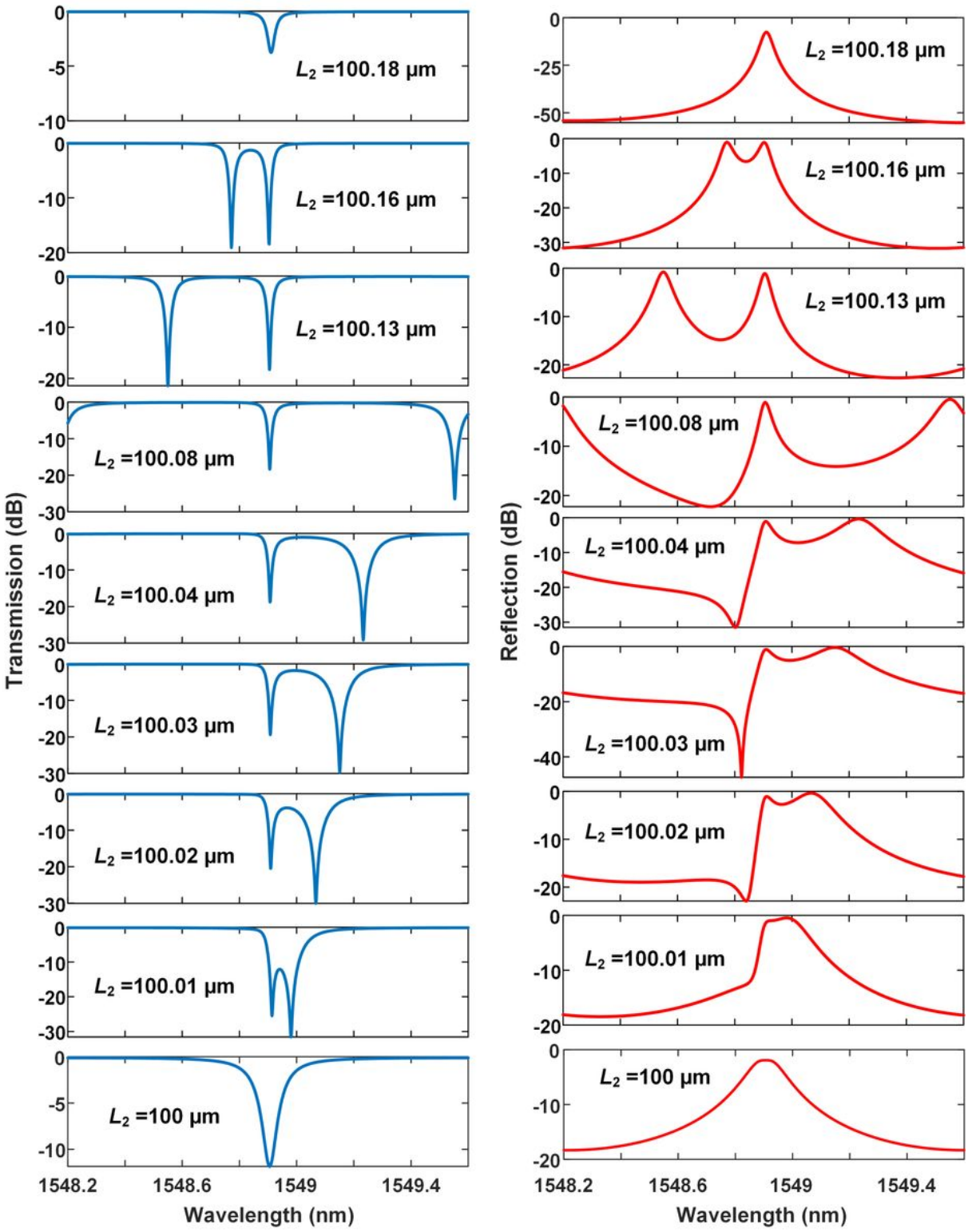

Figure 8

Power transmission (left) and reflection (right) spectra for various L_2. The structural parameters are t_{b1} = 0.83, t_{s1} = 0.707, t_{b2} = 0.98, t_{s2} = 0.707, L_{s1} = L_{s2} = 100 μm, L_1 = 200 μm, and L_3 = 100 μm.